

Bloch–Landau–Zener dynamics induced by a synthetic field in a photonic quantum walk

Cite as: APL Photonics **6**, 020802 (2021); <https://doi.org/10.1063/5.0037327>

Submitted: 12 November 2020 . Accepted: 27 January 2021 . Published Online: 24 February 2021

 Alessio D'Errico,  Raouf Barboza,  Rebeca Tudor,  Alexandre Dauphin,  Pietro Massignan,  Lorenzo Marrucci, and  Filippo Cardano

COLLECTIONS

Paper published as part of the special topic on [Synthetic Gauge Field Photonics](#)

 This paper was selected as Featured



View Online



Export Citation



CrossMark

ARTICLES YOU MAY BE INTERESTED IN

[Controlling the direction of topological transport in a non-Hermitian time-reversal symmetric Floquet ladder](#)

APL Photonics **6**, 010801 (2021); <https://doi.org/10.1063/5.0036494>

[Hybrid InP and SiN integration of an octave-spanning frequency comb](#)

APL Photonics **6**, 026102 (2021); <https://doi.org/10.1063/5.0035452>

[Simple method for mid-infrared optical frequency comb generation with dynamic offset frequency tuning](#)

APL Photonics **6**, 026103 (2021); <https://doi.org/10.1063/5.0038496>

APL Photonics

SPECIAL TOPIC: Coronavirus and Photonics

Submit Today!

Bloch–Landau–Zener dynamics induced by a synthetic field in a photonic quantum walk

Cite as: APL Photon. 6, 020802 (2021); doi: 10.1063/5.0037327

Submitted: 12 November 2020 • Accepted: 27 January 2021 •

Published Online: 24 February 2021



View Online



Export Citation



CrossMark

Alessio D’Errico,^{1,2,a)}  Raouf Barboza,¹  Rebeca Tudor,^{1,3}  Alexandre Dauphin,⁴  Pietro Massignan,^{4,5} 
Lorenzo Marrucci,^{1,6}  and Filippo Cardano^{1,a)} 

AFFILIATIONS

¹Dipartimento di Fisica “Ettore Pancini,” Università di Napoli Federico II, Complesso Universitario di Monte Sant’Angelo, Via Cintia, 80126 Napoli, Italy

²Department of Physics, University of Ottawa, 25 Templeton Street, Ottawa, Ontario K1N 6N5, Canada

³National Institute for Research and Development in Microtechnologies IMT, Bucharest 077190, Romania

⁴ICFO—Institut de Ciències Fotoniques, The Barcelona Institute of Science and Technology, 08860 Castelldefels (Barcelona), Spain

⁵Departament de Física, Universitat Politècnica de Catalunya, Campus Nord B4-B5, 08034 Barcelona, Spain

⁶CNR-ISASI, Institute of Applied Science and Intelligent Systems, Via Campi Flegrei 34, 80078 Pozzuoli (NA), Italy

Note: This paper is part of the APL Photonics Special Topic on Synthetic Gauge Field Photonics.

^{a)} **Authors to whom correspondence should be addressed:** aderrico@uottawa.ca and filippo.cardano2@unina.it

ABSTRACT

Quantum walks are processes that model dynamics in coherent systems. Their experimental implementations proved to be key to unveiling novel phenomena in Floquet topological insulators. Here, we realize a photonic quantum walk in the presence of a synthetic gauge field, which mimics the action of an electric field on a charged particle. By tuning the energy gaps between the two quasi-energy bands, we investigate intriguing system dynamics characterized by the interplay between Bloch oscillations and Landau–Zener transitions. When both gaps at quasi-energy values of 0 and π are vanishingly small, the Floquet dynamics follows a ballistic spreading.

© 2021 Author(s). All article content, except where otherwise noted, is licensed under a Creative Commons Attribution (CC BY) license (<http://creativecommons.org/licenses/by/4.0/>). <https://doi.org/10.1063/5.0037327>

I. INTRODUCTION

Quantum walks (QWs) are periodically driven processes describing the evolution of quantum particles (walkers) on a lattice or a graph.^{1,2} The walker evolution is determined by the unitary translation operators that, at each time step, couple the particle to its neighboring sites in a way that is conditioned by the state of an internal degree of freedom, referred to as “the coin.” An additional unitary operator acts on the internal degrees of freedom, therefore mimics the “coin tossing” of the classical random walk, and is usually referred to as *coin rotation*.¹ Besides the original interest in QWs for quantum computation,^{3–7} these processes have proved to be powerful tools to investigate topological systems,^{8–22} disordered systems and Anderson localization,^{23–26} and multiparticle interactions and correlations.^{27–29} QWs have been implemented in many different physical platforms: atoms in optical lattices,^{30,31} trapped ions,³²

Bose–Einstein condensates,³³ superconducting qubits in microwave cavities,¹⁴ and photonic setups.^{10,19,27,29,34–36} They exhibit peculiar properties when an external force acts on the walker, mimicking the effect of an electric field on a charged particle. These processes, baptized as “Electric Quantum Walks” in Ref. 31, have been studied theoretically in previous works^{37,38} and implemented using neutral atoms in optical lattices,³¹ photons,³⁹ and transmon qubits in optical cavities.¹⁴ Recently, these concepts have been generalized to 2D QWs.^{19,40} In this scenario, the walker dynamics can be remarkably different with respect to a standard QW evolution. While in the absence of a force the walker wavefunction spreads ballistically, by applying a constant force it is possible to observe revivals of the initial distribution at specific time steps.³¹ Electric QWs are thus an ideal platform to investigate spatial localization induced by “irrational forces,”^{31,38,41} revivals of probability distributions^{41–45} and can be used to detect topological invariants.^{14,19,46–49}

Similar to a quantum particle in a periodic potential, in the presence of a constant force, the walker trajectory performs Bloch oscillations (BO) as a consequence of the particle momentum being a periodic quantity.^{50–52} In quantum walks, BOs manifest directly when the input wavepacket approximates one of the system eigenstates, as first observed in Ref. 53. However, for generic initial conditions, collective BOs of the excited eigenstates may lead to a revival of the whole probability distribution at periodic intervals of time.^{39,40,48} Revivals can be observed only in the case of forces that are much smaller than the relevant energy gap. These effects can be indeed destroyed by Landau–Zener transitions, occurring when a fraction of the wavepacket is transferred to a band different from the initial one.^{48,54}

In the continuous time regime, it is well known that the interplay between Landau–Zener transitions and Bloch oscillations manifests itself in processes with two characteristic periods⁵² that, under specific circumstances, may lead to breathing phenomena even when interband transitions are not negligible. In our work, we make use of a novel platform, which exploits the space of transverse momentum of a paraxial light beam,¹⁹ to generate electric QWs, with the possibility of tuning both the force strength and the energy gap size. With this setup, we observe revivals due to either Bloch oscillations or multiple Landau–Zener transitions. Finally, we discuss how the Floquet nature of these systems affects the walker dynamics. In particular, when the two energy gaps in the spectrum are sufficiently small, the number of LZ transitions is doubled within a single period. This, in turn, causes the appearance of multiple trajectories, arranged in peculiar regular patterns.

This paper is structured as follows: In Sec. II, we describe our photonic quantum walk, defining the quantum evolutions that we investigated both numerically and experimentally. In Sec. III, we discuss the implementation of a synthetic electric field. In Sec. IV, we illustrate theoretical aspects of BOs, revivals, and LZ transitions in our quantum walk, accompanied by numerical simulations. In Sec. V, we show that this QW can be engineered so as to feature two LZ transitions within a single period, exploiting the spectrum periodicity that is unique to Floquet systems. In Sec. VI, we report the experimental observation of refocusing effects and their interplay with LZ transitions. In Sec. VII, we draw our conclusions.

II. QUANTUM WALK IN THE MOMENTUM SPACE OF LIGHT

To simulate a QW on a one-dimensional lattice, we encode the walker into the transverse momentum of a paraxial light beam. In particular, the walker position, which is identified by an integer coordinate m , is associated with the photonic spatial mode $|m\rangle$ given by

$$|m\rangle = A(x, y, z)e^{i[(\Delta k m)x + k_z z]}, \quad (1)$$

where k_z is the wavevector component along the z direction, Δk is a constant such that $\Delta k \ll k_z$, and A is a Gaussian spatial envelope with a beam waist w_0 . Modes described in Eq. (1) are standard Gaussian beams, propagating along a direction that is slightly tilted with respect to the z -axis.

At each time step, the evolution is performed by the successive application of a rotation W of the coin degree of freedom and a translation T that shifts the walker to the left or to the right depending on the coin state being $|L\rangle$ or $|R\rangle$. In our setup, both operators are implemented by liquid-crystal (LC) birefringent waveplates. Along these plates, the LC molecular orientation angle α is suitably patterned,⁵⁵ as shown in Fig. 1(a). Here, the operator T is obtained when the local orientation α of the optic axis increases linearly along x ,

$$\alpha(x, y) = \pi x/\Lambda + \alpha_0, \quad (2)$$

where Λ is the spatial periodicity of the angular pattern and α_0 is a constant, thereby forming a regular pattern reminiscent of a diffraction grating. This device has been originally named g -plate.¹⁹ In the basis of circular polarizations $|L\rangle = (1, 0)^T$ and $|R\rangle = (0, 1)^T$, the associated operator can be written as

$$T \equiv \begin{pmatrix} \cos(\delta/2) & i \sin(\delta/2)e^{-2i\alpha_0} \hat{t} \\ i \sin(\delta/2)e^{2i\alpha_0} \hat{t}^\dagger & \cos(\delta/2) \end{pmatrix}, \quad (3)$$

where \hat{t} and \hat{t}^\dagger are the (spin-independent) left and right translation operators along x , acting as $\hat{t}|m, \phi\rangle = |m-1, \phi\rangle$ and $\hat{t}^\dagger|m, \phi\rangle = |m+1, \phi\rangle$, respectively, on the spatial modes in Eq. (1). Here, $|\phi\rangle$ is a generic polarization state and δ is the LC optical retardation, which can be tuned by adjusting the amplitude of an alternating

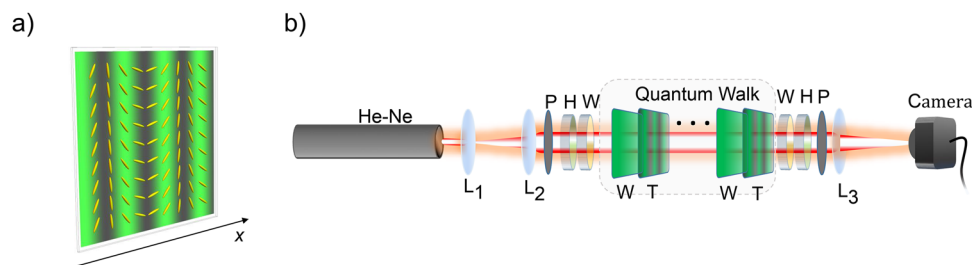


FIG. 1. Scheme of the experimental setup. (a) Schematic illustration of a g -plate. The ellipsoids show the local orientation of the liquid crystal molecules; the background pattern corresponds to the intensity of white light transmitted by crossed polarizers when a g -plate is placed between them. (b) Sketch of the experimental apparatus. A He–Ne laser beam is expanded by using two lenses (L_1 and L_2). The input polarization is adjusted by using a polarizer (P), a half-waveplate (H), and a quarter-waveplate (W). The QW is performed by alternating g -plates (T) and quarter waveplates (W). An optical 2D Fourier transform is performed on the final state by a converging lens. In its focal plane, the light intensity distribution is recorded by a camera. An additional stage (W–H–P) can be inserted before lens L_3 to analyze a single polarization/coin component.

voltage applied to the cell.⁵⁶ The coin rotation is realized by uniform LC plates ($\alpha = 0$), represented by the operator

$$L(\delta) = \begin{pmatrix} \cos(\delta/2) & i \sin(\delta/2) \\ i \sin(\delta/2) & \cos(\delta/2) \end{pmatrix}. \quad (4)$$

Typically, we set $\delta = \pi/2$ so as to obtain a standard quarter-waveplate, $W = L(\pi/2)$. The quantum walk is realized by applying repeatedly the single step unitary process

$$U_0(\delta, \alpha_0) = T(\delta, \alpha_0) \cdot W, \quad (5)$$

and the state after t steps is given by $|\psi(t)\rangle = U_0^t |\psi(0)\rangle$.

Relying on this approach, we realize our QW in the setup sketched in Fig. 1(b). A coherent light beam (produced by a He:Ne laser source, with wavelength $\lambda = 633$ nm), whose spatial envelope is that of a Gaussian mode, is initially expanded to reach a waist $w_0 \simeq 5$ mm. After preparing the desired beam polarization with a polarizer (P), a half-waveplate (H), and a quarter-waveplate (W), we perform the quantum walk by letting the beam pass through a sequence of g -plates (T) and quarter-waveplates. In the present experiment, we realized walks containing 14 unit steps. The optical retardation of the g -plates is controlled by tuning an alternating voltage, and their spatial period is $\Lambda = w_0 = 5$ mm. As explained in detail in Ref. 19, with this choice of parameters, we simulate the evolution of an initial state that is localized in the transverse wavevector space, corresponding to the spatial mode $|m\rangle = 0$. All the devices that implement the QW are liquid crystal plates, fabricated in our

laboratories and mounted in a compact setup. The final probability distribution is extracted from the intensity distribution in the focal plane of a converging lens located at the end of the QW.¹⁹ This distribution consists of an array of Gaussian spots, centered on the lattice sites, whose relative power (normalized with respect to the total power) gives the corresponding walker probabilities. An additional set of waveplates and a polarizer can be placed before the lens to analyze specific polarization components. We use these projections to prove that, when a substantial revival of the probability distribution is observed, the coin part of the final state corresponds to the initial one.

III. REALIZING AN ELECTRIC QW

The discrete translational symmetry in the walker space implies that the unitary single step operator U_0 can be block-diagonalized in the quasi-momentum basis,⁸

$$U_0 = \int_{-\pi}^{\pi} \frac{dq}{2\pi} \mathcal{U}_0(q) \otimes |q\rangle\langle q|, \quad (6)$$

where $|q\rangle = \sum_m e^{iqm} |m\rangle$, with q varying in the first Brillouin zone $BZ = [-\pi, \pi]$. In the case of a 2D coin space, the operator $\mathcal{U}_0(q)$ is a 2×2 unitary matrix, which may be written as

$$\mathcal{U}_0(q) = \exp[-iE(q)\mathbf{n}(q) \cdot \boldsymbol{\sigma}], \quad (7)$$

where $\mathbf{n}(q)$ is a unit vector, $\boldsymbol{\sigma} = (\sigma_1, \sigma_2, \sigma_3)$ is the vector composed of the three Pauli matrices, and $\pm E(q)$ are the quasienergies of the two bands of the system⁸ [see Fig. 2(a)]. With the QW being

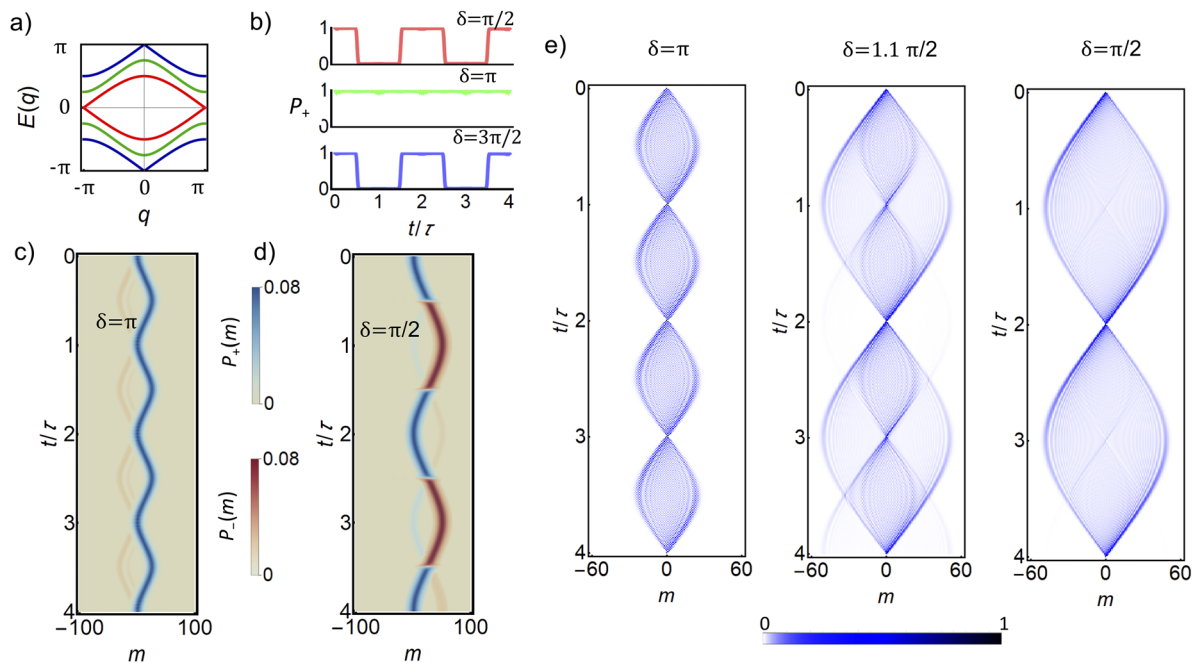


FIG. 2. Numerical simulations of electric quantum walks. (a) Quasi-energy dispersion $E(q)$ for various optical retardations: $\delta = \pi/2$ (red), $\delta = \pi$ (green), and $\delta = 3\pi/2$ (blue). [(b)–(d)] We simulate the evolution of broad wavepackets prepared in the upper band with a width $w = 10$ under an external force $F = \pi/50$. In panel (b), we plot the probability that the evolved state is located on the upper band. Panels (c) and (d) show the spatial probability distributions relative to the two bands [$P_+(m)$ and $P_-(m)$] as a function of the time step. (e) Evolutions of initially localized states generated during the QW dynamics under a force $F = \pi/50$ for three different values of δ . Localized inputs give rise to trajectories with multiple revivals. The initial state of these simulations is $|H\rangle|m=0\rangle = (|R\rangle + |L\rangle)|0\rangle/\sqrt{2}$.

a Floquet evolution, this spectrum exhibits two gaps at quasi-energies values of 0 and π . For practical reasons, we define the quantity E_g as the minimum value between the two gap sizes (when varying the quasi-momentum in the BZ). In the following, we will denote the eigenstates of the quantum walk evolution in the absence of an external force as $|u_{\pm}(q)\rangle \otimes |q\rangle$, where $|u_{\pm}(q)\rangle$ is the coin part. In this work, we implement QWs corresponding to two different regimes: $\delta = \pi$ and $\delta = \pi/2$. In the first case, E_g is at its maximum value, providing the optimal configuration for the observation of clean Bloch oscillations. In the second case, the gap at $E = 0$ vanishes [see Fig. 2(a)]. In this case, a LZ transition occurs with unit probability.

As discussed in previous works,^{19,31} applying an external constant force F is equivalent to shifting linearly in time the quasi-momentum: $q(t) = q(0) + Ft$. Hence, the single step operator at the time step t , labeled $\mathcal{U}(q, t)$, satisfies the following equation:

$$\mathcal{U}(q, t) = \mathcal{U}_0(q + Ft). \quad (8)$$

In our setup, the walker position is encoded into the optical transverse wavevector. As such, the walker quasi-momentum corresponds to the spatial coordinate x in our laboratory reference frame, introduced to define spatial modes in Eq. (1). In particular, x and q are related by the following expression:¹⁹

$$q = -\frac{2\pi x}{\Lambda}. \quad (9)$$

Using Eqs. (8) and (9), it is straightforward to see that the effect of a constant force is simulated if the g -plates corresponding to the time step t are shifted along x by the amount $\Delta x_t = t \Lambda F / (2\pi)$.

IV. REFOCUSING EFFECTS IN ELECTRIC QUANTUM WALKS

Bloch oscillations have been extensively studied in the continuous time regime (see Refs. 57 and 58) and have been recently considered in discrete time settings.^{42,59} Here, we review the theory of Bloch oscillations and Landau-Zener transitions and investigate their phenomenology in our quantum walk protocol.

Consider the evolution of an initial state that approximates an eigenstate of the system without any force, namely, a Gaussian wavepacket centered around $m = 0$,

$$|\Psi(q_0, w)\rangle = \mathcal{N} \sum_m \exp[-(m/w)^2 + iq_0 m] |u_{\pm}(q_0)\rangle \otimes |m\rangle, \quad (10)$$

where \mathcal{N} is a normalization factor and w controls the width of the wave packet. We consider wavepackets with large values of w so that these states are sharply peaked in quasi-momentum space. If the external force F is small with respect to the minimum energy gap, the adiabatic approximation dictates that (i) the wavepacket remains in the original quasi-energy band during the whole evolution, (ii) the coin state rotates as $|u_{\pm}(q_0)\rangle \rightarrow |u_{\pm}(q_0 + Ft)\rangle$, and (iii) the center of mass follows the equation of motion: $m(t) = (1/F) \int_{q_0}^{q_0 + Ft} v_g(q) dq$, where $v_g(q) = \partial_q E_{\pm}(q)$ is the group velocity. In particular, after a period $\tau = 2\pi/F$, the wavepacket gets back to the original state. This result is illustrated in Figs. 2(b) and 2(c) for the case in which the initial state is in the upper band. In panel (b), we plot the probability that the walker is found in the upper energy band, which remains

approximately equal to one across the evolution. In panel (c), we report in a single plot the probability $P_{\pm}(m, t)$ that, at the time step t , the walker is found on the lattice site m in the upper (lower) band. A different scenario occurs for a closed energy gap (for instance, at $\delta = \pi/2$). In this case, the adiabatic approximation breaks up when the wavepacket reaches the region of the Brillouin zone where E_g is minimum. The Landau-Zener theory⁵⁴ predicts that the transition to the lowest band occurs with unit probability in the case of zero gap. We clearly observe this phenomenon in our simulations [see Figs. 2(b) and 2(d)]. After a period τ , the wavepacket is entirely found in the lowest band as a consequence of a LZ transition. However, at $t = 2\tau$, a second transition takes place and the input state is restored. Remarkably, the same dynamics is observed for $\delta = 3\pi/2$, where the gap between the two bands vanishes at $E(q = 0) = \pm\pi$. Such a situation can only appear in a Floquet system.

Observing the dynamics of Gaussian wavepackets facilitates the understanding of the evolution of localized input states, which are not confined to a single band. In this situation, the oscillating behavior of the system eigenstates can lead to a refocusing of the localized input. To illustrate this result, let us consider a generic initial state,

$$|\psi_0\rangle = \int_{-\pi}^{\pi} \frac{dq}{2\pi} [c_+(q)|u_+(q)\rangle + c_-(q)|u_-(q)\rangle] \otimes |q\rangle. \quad (11)$$

The state after τ steps is given by

$$|\psi_{\tau}\rangle = \int_{-\pi}^{\pi} \frac{dq}{2\pi} \prod_{t=0}^{\tau} \mathcal{U}_0(q + Ft) \times [c_+(q)|u_+(q)\rangle + c_-(q)|u_-(q)\rangle] \otimes |q\rangle, \quad (12)$$

where the product $\prod_{t=0}^{\tau} \mathcal{U}_0(q + Ft)$ must be written in the time ordered form. In the adiabatic regime where $F \ll E_g$, we find (see Appendix A for details)

$$|\psi_{\tau}\rangle = \int_{-\pi}^{\pi} \frac{dq}{2\pi} \left(c_+(q) e^{-i(\gamma_+ + \gamma_g)} |u_+(q)\rangle + c_-(q) e^{-i(\gamma_- + \gamma_g)} |u_-(q)\rangle \right) \otimes |q\rangle. \quad (13)$$

The Zak phase γ_g ⁶⁰ appears as a global phase and does not play an important role here. We rather focus our attention to the dynamical phases acquired by the eigenstates when undergoing a complete Bloch oscillation, which are given by

$$\gamma_{\pm} = \sum_{j=0}^{(2\pi/F)-1} E_{\pm}(q + jF). \quad (14)$$

These phases are independent of q in the limit of small F , and hence, they can be factored out from the integrals. Therefore, if at $t = 0$, only one band is occupied, the final state coincides with the initial one apart from a global phase factor. When the system is initially prepared in a state occupying both bands, complete refocusing can be observed when the difference between the dynamical phases, $\Delta\gamma = \gamma_+ - \gamma_-$, is a multiple of 2π . In general, the final state will be different from the initial one due to the additional relative phase acquired by the states over the two bands. In particular, for $\Delta\gamma = \pi$, the final state is orthogonal to the initial one, even though it is still localized at the initial lattice site.

At $\delta = \pi$, the difference $\Delta\gamma$ is 2π for $F = 2\pi/2l$, with l being an integer, and π for $F = 2\pi/(2l + 1)$. In the first case, we can observe

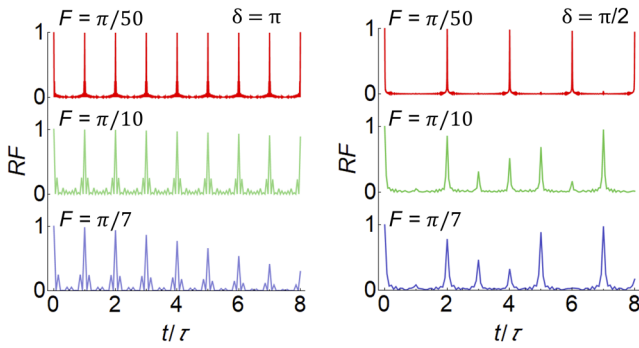


FIG. 3. Numerical simulations of the refocusing fidelity. Values of the RF calculated during the evolution for various strengths of the force F . In the left column, the optical retardation is set to $\delta = \pi$. The large spectral gap inhibits LZ transitions so that the system performs clean Bloch oscillations with very large RF. In the right column, δ is set to $\pi/2$ so that the spectral gap is closed. Very weak forces (red line) induce an almost perfect refocusing at twice the Bloch period τ .

refocusing of the full quantum state after a number of steps that is a multiple of $\tau = 2\pi/F$, as shown in Fig. 2(e). For a vanishing gap, this description breaks down in proximity of the gap-closing point. However, also in this case, a refocusing of the input state can be observed at time step multiples of 2τ as a result of the even number of Landau–Zener transitions occurring for each eigenstate^{54,61} [see Fig. 2(d)]. This is confirmed by the results of numerical simulations reported in Fig. 2(e) for a QW with $\delta = \pi/2$. The evolution at $\delta = 3\pi/2$ is actually identical to the latter case. Indeed, the two single step operators are the same, apart from a global phase factor $\exp(i\pi)$ and a π shift of the whole BZ.

A quantitative analysis of non-adiabatic effects in QWs with $\delta = \pi$ and $\delta = \pi/2$ is provided in Fig. 3, depicting the refocusing fidelity $RF = |\langle \psi(n\tau) | \psi(0) \rangle|^2$. When $\delta = \pi$, the RF is peaked at $t = n\tau$, and it is approximately equal to one for small values of the force, while the peak value decreases with the increase in F . In the case $\delta = \pi/2$, for small values of the force ($F = \pi/50$), a good refocusing is observed at $t = 2n\tau$ (with n integer). For stronger forces (e.g., $F = \pi/10$ and $F = \pi/7$), the behavior at longer times appears more complicated due to the effect of residual Bloch oscillations responsible for the peaks at odd multiples of τ .

V. DOUBLE LZ TRANSITIONS WITHIN A SINGLE OSCILLATION PERIOD

Before discussing the experimental results, we illustrate an additional QW dynamics in the very peculiar case where both energy gaps at $E = 0$ and $E = \pi$ are made small so that LZ can take place with high probability twice when crossing the Brillouin zone. This is a unique feature of Floquet systems. We consider a protocol defined by the single step operator $U_0(\delta) = T(\pi)L(\delta)$. In Fig. 4(a), we plot the quasi-energy spectrum for three values of δ . The minimum energy gaps around $E = 0$ and $E = \pi$ are located at quasi-momentum values $q = 0$ and $q = \pi$, respectively, and have the same amplitude. Their value can be tuned by adjusting δ . Figure 4(b) depicts the walker evolution in the case $\delta = 0.9\pi$, considering as the input state a wavepacket entirely localized on the upper band. It is clear that

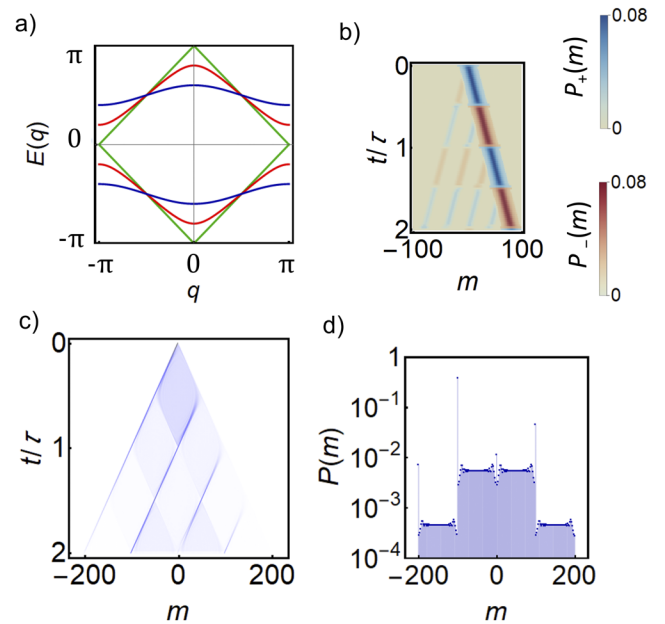


FIG. 4. Numerical simulations of double LZ transitions within a single oscillating period. (a) Quasi-energy spectrum of the protocol $U_0(\delta)$ for three values of δ : $\delta = 0.5\pi$ (blue), $\delta = 0.7\pi$ (red), and $\delta = 0.9\pi$ (green); (b) Gaussian wavepacket evolution [$F = \pi/20$ and $\delta = 0.9\pi$]. As in Fig. 2, the wavepacket is prepared with a width $w = 10$ and coin corresponding to the upper band eigenstate at $q = 0$. The plot shows simultaneously the probability distributions relative to the upper and lower band. (c) Localized input state [$F = \pi/50$ and $\delta = 0.9\pi$; initial coin state: $|H\rangle$]. (d) Total probability distribution at $t = 200$.

within a single period τ two LZ transitions take place. The fraction of the wavepacket that undergoes two transitions keeps moving in the same direction, as its group velocity does not change sign. Figure 4(c) shows the evolution in the case of a localized input state. Also in this case, at each transition, the wavepacket splits into a component that keeps moving in the same direction and another that is reflected, similarly to a beam splitter. The interplay between these two mechanisms gives rise to a complex dynamics, where at each period τ the wavepacket is concentrated on a set of lattice sites that are equally spaced, as shown in Fig. 4(d).

VI. EXPERIMENTAL RESULTS

We benchmark our platform by first performing experiments of QWs without an external force. The results are reported in Fig. 5(a), showing the well-known ballistic propagation that characterizes these processes.⁶² Experimental probability distributions $|\psi_E(m)|^2$ are compared with theoretical simulations $|\psi_T(m)|^2$, with their agreement being quantified by the similarity⁶³

$$S = \sqrt{\frac{\sum_m |\psi_E(m)|^2 |\psi_T(m)|^2}{\sum_m |\psi_E(m)|^2 \sum_m |\psi_T(m)|^2}}, \quad (15)$$

where we are assuming that $|\psi_E(m)|^2$ and $|\psi_T(m)|^2$ are normalized. In Figs. 5 and 6, we report the similarity S averaged over the results for each step. All the experimental errors were obtained by repeating each experiment four times.

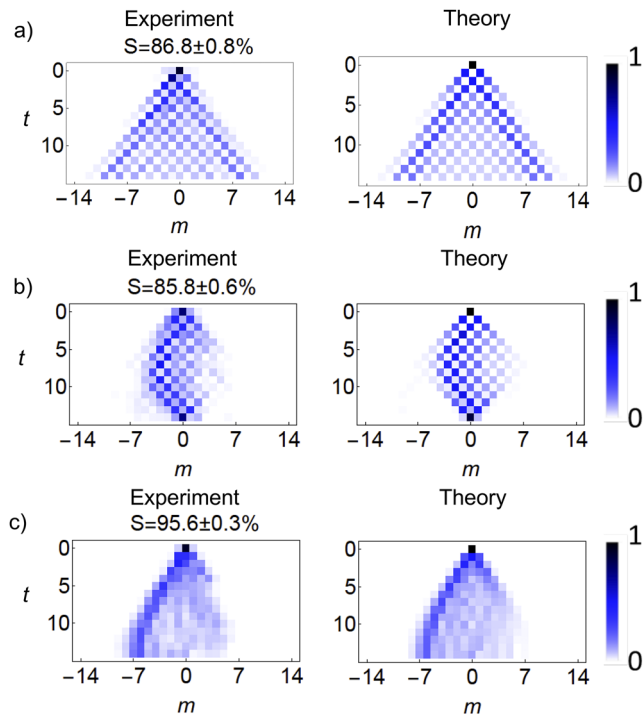


FIG. 5. Experimental demonstration of revivals in electric QWs. We plot the walker probability distributions of electric quantum walks (14 steps) with or without an applied force. Experimental and theoretical results are reported in the left and right panels, respectively. A quantitative comparison is provided in terms of the similarities. (a) $\delta = \pi$ and $F = 0$. (b) $\delta = \pi$ (energy gap is maximum) and $F = \pi/7$. (c) $\delta = \pi/2$ (energy gap is vanishing) and $F = \pi/7$. The coin input state is $|\psi(0)\rangle = |H, m = 0\rangle = (|L\rangle + |R\rangle)|0\rangle/\sqrt{2}$. Experimental data are averages over four repeated measurements.

To confirm experimentally the results discussed in Sec. IV, in Fig. 5(b) we show an electric quantum walk characterized by a force $F = \pi/7$. Here, a complete refocusing is observable at the time step $t = 14$, corresponding to the last step of our evolution. The evolution corresponds to the case $\delta = \pi$ so that the force is still smaller than the energy gap, even if interband transitions are not completely negligible. Besides being mostly localized at $m = 0$, the final state is expected to have the same polarization of the input beam, since refocusing happens after an even number of steps. Defining $|\phi_\tau\rangle$ as the polarization state measured for the optical mode with $m = 0$ after τ steps, we calculated the coin refocusing fidelity $R = |\langle\phi_0|\phi_\tau\rangle|^2$ (not to be confused with the refocusing fidelity of the whole quantum state RF considered in Fig. 3) that measures the overlap between the two coin states. We obtain $R > 98\%$ for three different input states, as shown in Appendix B. This is in agreement with the adiabatic model we developed earlier, where we showed that, for $F = 2\pi/\tau$, with τ being an even number, the initial state is fully reconstructed after τ steps.

The contribution of Bloch oscillations is completely suppressed for $\delta = \pi/2$, where the energy spectrum presents a gap closing point and the revival of the input state cannot occur. This is shown in

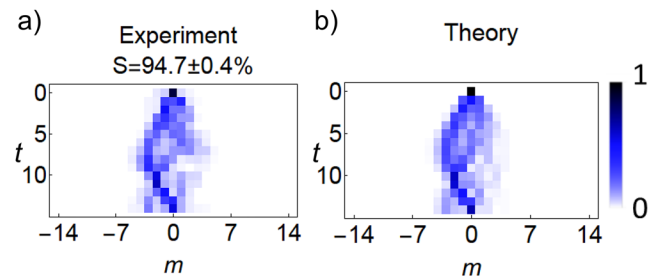


FIG. 6. Nonadiabatic refocusing. We realize 14 steps of an electric quantum walk with force $F = 2\pi/7$ such that the Brillouin Zone is explored twice. At $\delta = \pi/2$, due to the gap closing at $q = \pi$, Landau–Zener transitions occur with approximately unit probability. Hence, a double LZ transition should bring the particle to its original state. This is confirmed by our experiments [panel (a)], which are in good agreement with theoretical simulations [panel (b)]. Plots are shown for an H -polarized input state. Experimental data are averages over four repeated measurements.

the evolution depicted in Fig. 5(c). After 28 steps, an approximate refocusing is expected due to double Landau–Zener transitions (see Sec. IV). To observe this effect in our apparatus, we doubled the value of the force, that is, $F = 2\pi/7$. The results are shown in Fig. 6. After 14 steps, the wavefunction is again sharply peaked at the origin, with some broadening in agreement with numerical simulations. Refocusing in the regime of LZ transitions has been observed in the continuous time domain in bent waveguide arrays,⁵² but not in Floquet systems like ours.

VII. CONCLUSIONS

In this work, we studied electric QWs in one spatial dimension, relying on a platform where the walker degree of freedom is encoded in the transverse wavevector of a paraxial light beam.¹⁹ The presence of an external force is mimicked by applying a step-dependent lateral displacement of the liquid-crystal plates, increasing linearly with the step number. By tuning the energy gap of our system, we studied experimentally the interplay between Bloch oscillations and Landau–Zener transitions, which influence the emerging of revival of the input distribution of the walker wave packet. This allowed us to show experimentally that Landau–Zener oscillations, i.e., a revival of the probability distribution due to multiple Landau–Zener tunneling (already demonstrated in the continuous time regime⁵²), can be observed in discrete-time processes. Moreover, we investigated a regime with two transitions in a single Bloch oscillation by tuning the two gaps of our QW at $E = 0, \pi$, which is a possibility unique of Floquet systems. We plan to extend these studies to the regime of irrational forces and to study their interplay with static and dynamic disorder. Moreover, we aim to realize similar experiments in a two dimensional system with the same technology.¹⁹ Interesting phenomena could be observed by feeding our system with quantum light, investigating two photon interference induced by Bloch oscillations⁶⁴ or bunching and antibunching effects on NOON states.^{65,66} Furthermore, recent theoretical results predict peculiar effects for electric quantum walks in the non-Hermitian regime,⁶⁷ where Landau Zener tunneling can occur irreversibly, contrary to what happens in Hermitian systems.

ACKNOWLEDGMENTS

The authors thank M. Maffei and C. Esposito for their valuable help in the early stage of this project. A.D.'E., R.B., L.M., and F.C. acknowledge financial support from the European Union Horizon 2020 programme under European Research Council [ERC, Grant No. 694683 (PHOSPHOR)]. A.D.'E. acknowledges support by Ontario's Early Research Award (ERA), Canada Research Chairs (CRC), and the Canada First Research Excellence Fund (CFREF). R.T. acknowledges financial support from the IMT-Bucharest Core Program "MICRO-NANO-SIS-PLUS" 14N/2019 (Project No. PN 19160102) funded by MCE and from a grant of the Romanian Ministry of Research and Innovation, PCCDI-UEFISCDI (Project No. PN-III-P1-1.2-PCCDI-2017-0338/79PCCDI/2018) within PNCDI III. A.L.D. acknowledges financial support from the European Union Horizon 2020 program, under European Research Council (ERC) Advanced Grant (AdG) NOQIA (Grant No. 833801) and the FET-OPEN OPTOLoGic (Grant No. 899794), from the the Spanish Ministry of Economy and Competitiveness under the Severo Ochoa program for Centres of Excellence in RD (Grant No. CEX2019-000910-S) and under the Plan National FISCATEAMO and FIDEUA PID2019-106901GB-I00/10.13039/501100011033, Formation de personal investigador (FPI), from the Generalitat de

Catalunya under the AGAUR Grant (No. 2017 SGR 1341), the CERCA program and the QuantumCAT U16-011424 (co-funded by ERDF Operational Program of Catalonia 2014-2020), from the MINECO-EU QUANTERA MAQS (funded by State Research Agency (AEI) (PCI2019-111828-2/10.13039/501100011033), and from the National Science Centre, Poland-Symfonia (Grant No. 2016/20/W/ST4/00314). A.L.D. also acknowledges financial support from the following private foundations: the Fundacio Privada Cellex, Fundacio Mir-Puig, and the La Caixa Foundation (ID 100010434, fellowship code LCF/BQ/PR20/11770012).

APPENDIX A: DERIVATION OF EQ. (13)

The operators $\mathcal{U}(q + Ft)$ can be decomposed as

$$\mathcal{U}_0(q_t) = e^{iE(q_t)}|u_+(q_t)\rangle\langle u_+(q_t)| + e^{-iE(q_t)}|u_-(q_t)\rangle\langle u_-(q_t)|, \quad (\text{A1})$$

where we have defined $q_t = q + Ft$. In the adiabatic approximation, we have $\langle u_{\pm}(q_{t+1})|u_{\mp}(q_t)\rangle \ll 1$, i.e., interband transitions between successive steps happen with low probability. Within this approximation, the whole unitary evolution can be approximated by retaining the terms up to the first order in F ,

$$\begin{aligned} \prod_{t=0}^{\tau} \mathcal{U}_0(q + Ft) &= \left(e^{iE(q_{\tau})}|u_+(q_{\tau})\rangle\langle u_+(q_{\tau})| + e^{-iE(q_{\tau})}|u_-(q_{\tau})\rangle\langle u_-(q_{\tau})| \right) \times \dots \\ &\quad \times \left(e^{iE(q_0)}|u_+(q_0)\rangle\langle u_+(q_0)| + e^{-iE(q_0)}|u_-(q_0)\rangle\langle u_-(q_0)| \right) \\ &\approx e^{i\sum_{t=0}^{\tau} E(q_t)}|u_+(q_{\tau})\rangle\langle u_+(q_{\tau})|u_+(q_{\tau-1})\rangle \times \dots \times \langle u_+(q_1)|u_+(q_0)\rangle\langle u_+(q_0)| \\ &\quad + e^{-i\sum_{t=0}^{\tau} E(q_t)}|u_-(q_{\tau})\rangle\langle u_-(q_{\tau})|u_-(q_{\tau-1})\rangle \times \dots \times \langle u_-(q_1)|u_-(q_0)\rangle\langle u_-(q_0)| + U_{LZ} \\ &= e^{i\sum_{t=0}^{\tau} E(q_t)}|u_+(q_0)\rangle\langle u_+(q_0)| \left(\prod_{t=1}^{\tau} \langle u_+(q_t)|u_+(q_{t-1})\rangle \right) \\ &\quad + e^{-i\sum_{t=0}^{\tau} E(q_t)}|u_-(q_0)\rangle\langle u_-(q_0)| \left(\prod_{t=1}^{\tau} \langle u_-(q_t)|u_-(q_{t-1})\rangle \right) + U_{LZ}, \end{aligned} \quad (\text{A2})$$

where we used $q_0 = q_{\tau}$. In the limit of small F , the contributions $(\prod_{t=1}^{\tau} \langle u_{\pm}(q_t)|u_{\pm}(q_{t-1})\rangle)$ are equal to $\exp(i\gamma_z^{\pm})$, where γ_z^{\pm} are the Zak phases^{60,68} associated with the single energy bands. In our QW, $\gamma_z^+ = \gamma_z^- = \gamma_z$. The term U_{LZ} is an $O(F)$ contribution related to interband transitions. In the following, we show that its amplitude is negligible for $F \ll E_g$, where E_g is the energy gap defined in the main text (see also Ref. 14).

Let us evaluate explicitly U_{LZ} in order to show that it is negligible in the adiabatic approximation. U_{LZ} is given, to order $O(F)$, by a sum $U_{LZ} = \sum_{t^*=0}^{\tau} U_{LZ}(t^*)$, where $U_{LZ}(t^*)$ describes a process where a single Landau-Zener transition happens at $q = q_{t^*}$,

$$U_{LZ}(t^*) = |u_+(q_0)\rangle\langle u_-(q_0)| \left(\prod_{t=t^*+1}^{\tau} \langle u_+(q_{t+1})|u_+(q_t)\rangle e^{-iE(q_t)} \right) \langle \partial_q u_+(q_{t^*})|u_-(q_{t^*})\rangle F \left(\prod_{t=0}^{t^*-1} \langle u_-(q_{t+1})|u_-(q_t)\rangle e^{iE(q_t)} \right). \quad (\text{A3})$$

The $O(F)$ contributions to U_{LZ} are obtained setting $\langle u_{\pm}(q_{t+1})|u_{\pm}(q_t)\rangle \approx 1$,

$$U_{LZ} = |u_+(q_0)\rangle\langle u_-(q_0)| \left(\sum_{t^*=0}^{\tau} e^{-i\gamma_z^+} e^{2i\sum_{t=0}^{t^*} E(q_t)} \langle \partial_q u_+(q_{t^*})|u_-(q_{t^*})\rangle \right) F + (u_+ \leftrightarrow u_-). \quad (\text{A4})$$

From this result, it follows that the probability of a Landau-Zener transition is

$$P_{+-} = F^2 \left| \sum_{t^*=0}^{\tau} e^{2i\sum_{t=0}^{t^*} E(q_t)} \langle \partial_q u_+(q_{t^*})|u_-(q_{t^*})\rangle \right|^2. \quad (\text{A5})$$

This formula corresponds to the one found in Ref. 14. Within the approximations considered ($F \ll E_g$), P_{+-} is negligible (see also Ref. 14 for split-step quantum walk protocols). In particular, we have $P_{+-} < 0.1$ at $\delta = \pi$ for $F < \pi/7$. In this regime, we can thus discard the term U_{LZ} , and substituting Eq. (A2) in Eq. (12), we obtain Eq. (13).

APPENDIX B: EXPERIMENTAL DATA FOR THE EVALUATION OF REFOCUSING FIDELITY

To show that, for $\delta = \pi$, the measured central spot of the final probability distribution has the same polarization as the input state, we measured the projections on the three mutually unbiased bases: $\{|H\rangle, |V\rangle\}$, $\{|A\rangle, |D\rangle\}$, and $\{|L\rangle, |R\rangle\}$, which allows us to reconstruct the full coin state. Here, $|A, D\rangle = (|L\rangle \mp |R\rangle)/\sqrt{2}$, and $|V\rangle = i(|L\rangle - |R\rangle)/\sqrt{2}$. We obtained $R = 98\% \pm 2\%$ for $|\psi(0)\rangle = |H, m=0\rangle$, $R = 99\% \pm 2\%$ for $|\psi(0)\rangle = (|L\rangle - i|R\rangle)|0\rangle/\sqrt{2}$, and $R = 99\% \pm 3\%$ for $|\psi(0)\rangle = |L\rangle|0\rangle$. Fidelities are calculated by using intensities recorded in a square of 4×4 pixels centered on the maximum of each spot.

DATA AVAILABILITY

The data that support the findings of this study are available from the corresponding authors upon reasonable request.

REFERENCES

- Y. Aharonov, L. Davidovich, and N. Zagury, "Quantum random walks," *Phys. Rev. A* **48**, 1687 (1993).
- V. Kendon, "Quantum walks on general graphs," *Int. J. Quantum Inf.* **04**, 791 (2006).
- N. Shenvi, J. Kempe, and K. B. Whaley, "Quantum random-walk search algorithm," *Phys. Rev. A* **67**, 052307 (2003).
- A. M. Childs and J. Goldstone, "Spatial search by quantum walk," *Phys. Rev. A* **70**, 022314 (2004).
- A. M. Childs, "Universal computation by quantum walk," *Phys. Rev. Lett.* **102**, 180501 (2009).
- A. M. Childs and W. van Dam, "Quantum algorithms for algebraic problems," *Rev. Mod. Phys.* **82**, 1 (2010).
- N. B. Lovett, S. Cooper, M. Everitt, M. Trevers, and V. Kendon, "Universal quantum computation using the discrete-time quantum walk," *Phys. Rev. A* **81**, 042330 (2010).
- T. Kitagawa, M. S. Rudner, E. Berg, and E. Demler, "Exploring topological phases with quantum walks," *Phys. Rev. A* **82**, 033429 (2010).
- T. Kitagawa, M. a. Broome, A. Fedrizzi, M. S. Rudner, E. Berg, I. Kassal, A. Aspuru-Guzik, E. Demler, and A. G. White, "Observation of topologically protected bound states in photonic quantum walks," *Nat. Commun.* **3**, 882 (2012).
- J. M. Zeuner, M. C. Rechtsman, Y. Plotnik, Y. Lumer, S. Nolte, M. S. Rudner, M. Segev, and A. Szameit, "Observation of a topological transition in the bulk of a non-Hermitian system," *Phys. Rev. Lett.* **115**, 040402 (2015).
- F. Cardano, M. Maffei, F. Massa, B. Piccirillo, C. de Lisio, G. De Filippis, V. Cataudella, E. Santamato, and L. Marrucci, "Dynamical moments reveal a topological quantum transition in a photonic quantum walk," *Nat. Commun.* **7**, 11439 (2015).
- F. Cardano, A. D'Errico, A. Dauphin, M. Maffei, B. Piccirillo, C. de Lisio, G. De Filippis, V. Cataudella, E. Santamato, L. Marrucci, M. Lewenstein, and P. Massignan, "Detection of Zak phases and topological invariants in a chiral quantum walk of twisted photons," *Nat. Commun.* **8**, 15516 (2017).
- S. Barkhofen, T. Nitsche, F. Elster, L. Lorz, A. Gábris, I. Jex, and C. Silberhorn, "Measuring topological invariants in disordered discrete-time quantum walks," *Phys. Rev. A* **96**, 033846 (2017).
- V. V. Ramasesh, E. Flurin, M. Rudner, I. Siddiqi, and N. Y. Yao, "Direct probe of topological invariants using Bloch oscillating quantum walks," *Phys. Rev. Lett.* **118**, 130501 (2017).
- X. Zhan, L. Xiao, Z. Bian, K. Wang, X. Qiu, B. C. Sanders, W. Yi, and P. Xue, "Detecting topological invariants in nonunitary discrete-time quantum walks," *Phys. Rev. Lett.* **119**, 130501 (2017).
- L. Xiao, X. Zhan, Z. H. Bian, K. K. Wang, X. Zhang, X. P. Wang, J. Li, K. Mochizuki, D. Kim, N. Kawakami, W. Yi, H. Obuse, B. C. Sanders, and P. Xue, "Observation of topological edge states in parity-time-symmetric quantum walks," *Nat. Phys.* **13**, 1117 (2017).
- C. Chen, X. Ding, J. Qin, Y. He, Y.-H. Luo, M.-C. Chen, C. Liu, X.-L. Wang, W.-J. Zhang, H. Li, L.-X. You, Z. Wang, D.-W. Wang, B. C. Sanders, C.-Y. Lu, and J.-W. Pan, "Observation of topologically protected edge states in a photonic two-dimensional quantum walk," *Phys. Rev. Lett.* **121**, 100502 (2018).
- B. Wang, T. Chen, and X. Zhang, "Experimental observation of topologically protected bound states with vanishing Chern numbers in a two-dimensional quantum walk," *Phys. Rev. Lett.* **121**, 100501 (2018).
- A. D'Errico, F. Cardano, M. Maffei, A. Dauphin, R. Barboza, C. Esposito, B. Piccirillo, M. Lewenstein, P. Massignan, and L. Marrucci, "Two-dimensional topological quantum walks in the momentum space of structured light," *Optica* **7**, 108 (2020).
- A. D'Errico, F. Di Colandrea, R. Barboza, A. Dauphin, M. Lewenstein, P. Massignan, L. Marrucci, and F. Cardano, "Bulk detection of time-dependent topological transitions in quenched chiral models," *Phys. Rev. Res.* **2**, 023119 (2020).
- L. Xiao, T. Deng, K. Wang, G. Zhu, Z. Wang, W. Yi, and P. Xue, "Non-Hermitian bulk-boundary correspondence in quantum dynamics," *Nat. Phys.* **16**, 761 (2020).
- B. Wang, T. Chen, and X. Zhang, "Observation of novel robust edge states in dissipative non-Hermitian quantum walks," *Laser Photonics Rev.* **14**, 2000092 (2020).
- A. Schreiber, K. N. Cassemiro, V. Potoček, A. Gábris, I. Jex, and C. Silberhorn, "Decoherence and disorder in quantum walks: From ballistic spread to localization," *Phys. Rev. Lett.* **106**, 180403 (2011).
- A. Crespi, R. Osellame, R. Ramponi, V. Giovannetti, R. Fazio, L. Sansoni, F. De Nicola, F. Sciarrino, and P. Mataloni, "Anderson localization of entangled photons in an integrated quantum walk," *Nat. Photon.* **7**, 322 (2013).
- J. M. Edge and J. K. Asboth, "Localization, delocalization, and topological transitions in disordered two-dimensional quantum walks," *Phys. Rev. B* **91**, 104202 (2015).
- N. C. Harris, G. R. Steinbrecher, M. Prabhu, Y. Lahini, J. Mower, D. Bunandar, C. Chen, F. N. C. Wong, T. Baehr-Jones, M. Hochberg, S. Lloyd, and D. Englund, "Quantum transport simulations in a programmable nanophotonic processor," *Nat. Photon.* **11**, 447 (2017).
- A. Peruzzo, M. Lobino, J. C. F. Matthews, N. Matsuda, A. Politi, K. Poullos, X.-Q. Zhou, Y. Lahini, N. Ismail, K. Wörhoff, Y. Bromberg, Y. Silberberg, M. G. Thompson, and J. L. O'Brien, "Quantum walks of correlated photons," *Science* **329**, 1500 (2010).
- A. Schreiber, A. Gábris, P. P. Rohde, K. Laiho, M. Štefanač, V. Potoček, C. Hamilton, I. Jex, and C. Silberhorn, "A 2D quantum walk simulation of two-particle dynamics," *Science* **336**, 55 (2012).
- L. Sansoni, F. Sciarrino, G. Vallone, P. Mataloni, A. Crespi, R. Ramponi, and R. Osellame, "Two-particle bosonic-fermionic quantum walk via integrated photonics," *Phys. Rev. Lett.* **108**, 010502 (2012).
- M. Karski, L. Forster, J.-M. Choi, A. Steffen, W. Alt, D. Meschede, and A. Widera, "Quantum walk in position space with single optically trapped atoms," *Science* **325**, 174 (2009).
- M. Genske, W. Alt, A. Steffen, A. H. Werner, R. F. Werner, D. Meschede, and A. Alberti, "Electric quantum walks with individual atoms," *Phys. Rev. Lett.* **110**, 190601 (2013).
- F. Zähringer, G. Kirchmair, R. Gerritsma, E. Solano, R. Blatt, and C. F. Roos, "Realization of a quantum walk with one and two trapped ions," *Phys. Rev. Lett.* **104**, 100503 (2010).

- ³³S. Dadras, A. Gresch, C. Groiseau, S. Wimberger, and G. S. Summy, "Quantum walk in momentum space with a Bose-Einstein condensate," *Phys. Rev. Lett.* **121**, 070402 (2018).
- ³⁴M. a. Broome, A. Fedrizzi, B. P. Lanyon, I. Kassal, A. Aspuru-Guzik, and A. G. White, "Discrete single-photon quantum walks with tunable decoherence," *Phys. Rev. Lett.* **104**, 153602 (2010).
- ³⁵A. Schreiber, K. N. Cassemiro, V. Potoček, A. Gábris, P. J. Mosley, E. Andersson, I. Jex, and C. Silberhorn, "Photons walking the line: A quantum walk with adjustable coin operations," *Phys. Rev. Lett.* **104**, 050502 (2010).
- ³⁶F. Cardano, F. Massa, H. Qassim, E. Karimi, S. Slussarenko, D. Paparo, C. de Lisio, F. Sciarrino, E. Santamato, R. W. Boyd, and L. Marrucci, "Quantum walks and wavepacket dynamics on a lattice with twisted photons," *Sci. Adv.* **1**, e1500087 (2015).
- ³⁷A. Wójcik, T. Łuczak, P. Kurzyński, A. Grudka, and M. Bednarska, "Quasiperiodic dynamics of a quantum walk on the line," *Phys. Rev. Lett.* **93**, 180601 (2004).
- ³⁸M. C. Bañuls, C. Navarrete, A. Pérez, E. Roldán, and J. C. Soriano, "Quantum walk with a time-dependent coin," *Phys. Rev. A* **73**, 062304 (2006).
- ³⁹P. Xue, R. Zhang, H. Qin, X. Zhan, Z. H. Bian, J. Li, and B. C. Sanders, "Experimental quantum-walk revival with a time-dependent coin," *Phys. Rev. Lett.* **114**, 140502 (2015).
- ⁴⁰H. Chalabi, S. Barik, S. Mittal, T. E. Murphy, M. Hafezi, and E. Waks, "Guiding and confining of light in a two-dimensional synthetic space using electric fields," *Optica* **7**, 506 (2020).
- ⁴¹C. Cedzich and R. F. Werner, "Revivals in quantum walks with a quasiperiodically-time-dependent coin," *Phys. Rev. A* **93**, 032329 (2016).
- ⁴²C. Cedzich, T. Rybár, A. H. Werner, A. Alberti, M. Genske, and R. F. Werner, "Propagation of quantum walks in electric fields," *Phys. Rev. Lett.* **111**, 160601 (2013).
- ⁴³P. Xue, H. Qin, B. Tang, and B. C. Sanders, "Observation of quasiperiodic dynamics in a one-dimensional quantum walk of single photons in space," *New J. Phys.* **16**, 053009 (2014).
- ⁴⁴L. A. Bru, M. Hinarejos, F. Silva, G. J. de Valcárcel, and E. Roldán, "Electric quantum walks in two dimensions," *Phys. Rev. A* **93**, 032333 (2015).
- ⁴⁵T. Nitsche, S. Barkhofen, R. Kruse, L. Sansoni, M. Štefaňák, A. Gábris, V. Potoček, T. Kiss, I. Jex, and C. Silberhorn, "Probing measurement-induced effects in quantum walks via recurrence," *Sci. Adv.* **4**, eaar6444 (2018).
- ⁴⁶M. Atala, M. Aidelsburger, J. T. Barreiro, D. Abanin, T. Kitagawa, E. Demler, and I. Bloch, "Direct measurement of the Zak phase in topological Bloch bands," *Nat. Phys.* **9**, 795 (2013).
- ⁴⁷D. A. Abanin, T. Kitagawa, I. Bloch, and E. Demler, "Interferometric approach to measuring band topology in 2D optical lattices," *Phys. Rev. Lett.* **110**, 165304 (2013).
- ⁴⁸E. Flurin, V. V. Ramasesh, S. Hacohen-Gourgy, L. S. Martin, N. Y. Yao, and I. Siddiqi, "Observing topological invariants using quantum walks in superconducting circuits," *Phys. Rev. X* **7**, 031023 (2017).
- ⁴⁹L. K. Upreti, C. Evain, S. Randoux, P. Suret, A. Amo, and P. Delplace, "Topological swing of Bloch oscillations in quantum walks," *Phys. Rev. Lett.* **125**, 186804 (2020).
- ⁵⁰K. Leo, P. H. Bolivar, F. Brüggemann, R. Schwedler, and K. Köhler, "Observation of Bloch oscillations in a semiconductor superlattice," *Solid State Commun.* **84**, 943 (1992).
- ⁵¹H. Sanchis-Alepuz, Y. A. Kosevich, and J. Sánchez-Dehesa, "Acoustic analogue of electronic Bloch oscillations and resonant zener tunneling in ultrasonic superlattices," *Phys. Rev. Lett.* **98**, 134301 (2007).
- ⁵²F. Dreisow, A. Szameit, M. Heinrich, T. Pertsch, S. Nolte, A. Tünnermann, and S. Longhi, "Bloch-Zener oscillations in binary superlattices," *Phys. Rev. Lett.* **102**, 076802 (2009).
- ⁵³A. Regensburger, C. Bersch, B. Hinrichs, G. Onishchukov, A. Schreiber, C. Silberhorn, and U. Peschel, "Photon propagation in a discrete Fiber network: An interplay of coherence and losses," *Phys. Rev. Lett.* **107**, 233902 (2011).
- ⁵⁴S. N. Shevchenko, S. Ashhab, and F. Nori, "Landau-Zener-Stückelberg interferometry," *Phys. Rep.* **492**, 1 (2010).
- ⁵⁵A. Rubano, F. Cardano, B. Piccirillo, and L. Marrucci, "Q-plate technology: A progress review [invited]," *J. Opt. Soc. Am. B* **36**, D70 (2019).
- ⁵⁶B. Piccirillo, V. D'Ambrosio, S. Slussarenko, L. Marrucci, and E. Santamato, "Photon spin-to-orbital angular momentum conversion via an electrically tunable q-plate," *Appl. Phys. Lett.* **97**, 241104 (2010).
- ⁵⁷T. Hartmann, F. Keck, H. J. Korsch, and S. Mossmann, "Dynamics of Bloch oscillations," *New J. Phys.* **6**, 2 (2004).
- ⁵⁸F. Domínguez-Adame, "Beyond the semiclassical description of Bloch oscillations," *Eur. J. Phys.* **31**, 639 (2010).
- ⁵⁹P. Arnault, B. Pepper, and A. Pérez, "Quantum walks in weak electric fields and Bloch oscillations," *Phys. Rev. A* **101**, 062324 (2020).
- ⁶⁰J. Zak, "Berry's phase for energy bands in solids," *Phys. Rev. Lett.* **62**, 2747 (1989).
- ⁶¹B. M. Breid, D. Witthaut, and H. J. Korsch, "Bloch-Zener oscillations," *New J. Phys.* **8**, 110 (2006).
- ⁶²J. Kempe, "Quantum random walks: An introductory overview," *Contemp. Phys.* **44**, 307 (2003).
- ⁶³T. Kailath, "The Divergence and Bhattacharyya distance measures in signal selection," *IEEE Trans. Commun.* **15**, 52 (1967).
- ⁶⁴S. Longhi, "Optical Bloch oscillations and zener tunneling with nonclassical light," *Phys. Rev. Lett.* **101**, 193902 (2008).
- ⁶⁵Y. Bromberg, Y. Lahini, and Y. Silberberg, "Bloch oscillations of path-entangled photons," *Phys. Rev. Lett.* **105**, 263604 (2010).
- ⁶⁶M. Lebugle, M. Gräfe, R. Heilmann, A. Perez-Leija, S. Nolte, and A. Szameit, "Experimental observation of N00N state Bloch oscillations," *Nature Commun.* **6**, 8273 (2015).
- ⁶⁷S. Longhi, "Non-Bloch-band collapse and chiral Zener tunneling," *Phys. Rev. Lett.* **124**, 066602 (2020).
- ⁶⁸M. V. Berry, "Quantal phase factors accompanying adiabatic changes," *Proc. R. Soc. A* **392**, 45 (1984).